25-29 August 2024
inter.noise
NANTES FRANCE

Virtual acoustic black holes as a means to achieve low-frequency vibration reduction

Samuel Quaegebeur[1]
Ecole Centrale de Lyon, CNRS, ENTPE, LTDS, UMR5513
Ecole Centrale de Lyon, 36 avenue Guy de Collongue 69130 Ecully, France

Ghislain Raze[2]
Liege University
University of Liège, Quartier Polytech 1 (B52/3), Allée de la Découverte 9, B-4000 Liège, Belgium

Li Cheng[3]
Hong Kong Polytechnic University
Department of Mechanical Engineering, The Hong Kong Polytechnic University, Hung Hom Kowloon, Hong Kong SAR, P. R. China

Gaëtan Kerschen[4]
Liege University
University of Liège, Quartier Polytech 1 (B52/3), Allée de la Découverte 9, B-4000 Liège, Belgium

ABSTRACT

Acoustic black holes (ABH) offer exceptional broadband vibration capabilities but have the inherent drawback of being only effective beyond a specific cut-on frequency. The most straightforward approach to set this threshold to a low value is to increase the ABH length. However, such a strategy leads to a very thin tip of the ABH, making it very complicated if not impossible to manufacture. Improving this ABH property has been for the past decade an active field of research. Recently, the concept of a virtual acoustic black (VABH) has been proposed by the authors. The key idea of this approach is to implement digitally the mechanical impedance of the ABH. The virtual feature of this strategy enables the implementation of any kind of ABH (any dimensions, material). Setting the cut-on frequency to low values thus becomes possible. The VABH is implemented through the use of piezoelectric patches, making it very compact and autonomous. Experimental demonstration shows that the proposed idea is able to mitigate vibration below 100 Hz.

1. INTRODUCTION

Initially proposed by Mironov in 1988 [1], the ABH has the inherent property to mitigate vibrations starting at a cut-on frequency determined by its geometry, and material [2]. For the past two

[1]samuel.quaegebeur@ec-lyon.fr

[2]g.raze@uliege.be

[3]li.cheng@polyu.edu.hk

[4]g.kerschen@uliege.be

decades, ABHs have been the subject of intense research [3]. One of the current main challenges is to reduce vibration levels at low frequencies. To achieve this goal, numerous developments have been proposed. Mechanical improvements were developed through extensions of the ABH [4] or spiral-shaped ABH [5] to name a few. Other research employed nonlinearities as a means to enhance the mitigation at low frequencies. In [6], the authors proposed to combine nonlinear vibration absorbers with the ABH effect. In [7]. an energy transfer from low to high frequencies was achieved through vibro-impact. Using the same nonlinear phenomena of energy transfer, Sun et al. [8] employed geometrical nonlinearities to achieve vibration mitigation at low frequencies. Recently, the ABH effect has been combined with electrical components to enhance its effect: in [9], a feedforward strategy is implemented, in [10] a shunt approach. Recently, the authors proposed an ABH concept that is entirely virtual (virtual ABH: VABH) [11]. The idea is to implement digitally the impedance of the ABH. Due to its virtual nature, any ABH can be realized. This offers countless possible designs including the one to select a very low cut-on frequency and thus to mitigate vibration for very low frequencies. This concept was then extended to be employed with piezoelectric patches, making it autonomous and self-contained [12]. This paper aims to show the benefits of such a design. First, Section 2 summarizes the theory of the VABH concept. Section 3 then presents experimental results. The test case considered for this study is a cantilever beam.

2. THEORY ON THE VIRTUAL IMPLEMENTATION OF THE ACOUSTIC BLACK HOLE

This section aims to review the theoretical background on the derivations of the VABH implemented with piezoelectric patches. For more details, the reader is referred to [12]. The key idea of the VABH is to ensure the equivalence between the system depicted in Figure 1 (beam with a mechanical ABH) and the one in Figure 2 (equipped only with piezoelectric patches). To this end, the equation of motion governing both systems must be identical.

2.1. Evaluation of the ABH impedance

The first step is to evaluate how the ABH modifies the uniform beam's dynamics. One possible methodology, considered herein, consists in deriving the ABH impedance through the finite element method. Here, a node is described by its longitudinal, vertical displacements but also by its rotation.

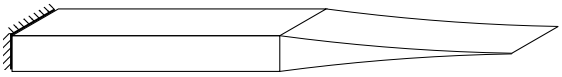

Figure 1: Cantilever beam with an ABH.

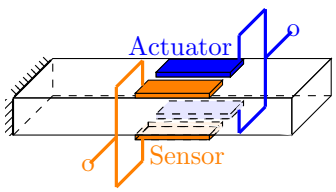

Figure 2: Cantilever beam with piezoelectric patches.

The superscripts b and tb denote the uniform and tapered wedge beams, respectively. The equations of motion read

$$\begin{bmatrix} \mathbf{M}^{\mathrm{b}}_{\mathrm{II}} & \mathbf{M}^{\mathrm{b}}_{\mathrm{IB}} \\ \mathbf{M}^{\mathrm{b}}_{\mathrm{BI}} & \mathbf{M}^{\mathrm{b}}_{\mathrm{BB}} \end{bmatrix} \begin{bmatrix} \ddot{\mathbf{x}}^{\mathrm{b}}_{\mathrm{I}} \\ \ddot{\mathbf{x}}_{\mathrm{B}} \end{bmatrix} + \begin{bmatrix} \mathbf{C}^{\mathrm{b}}_{\mathrm{II}} & \mathbf{C}^{\mathrm{b}}_{\mathrm{IB}} \\ \mathbf{C}^{\mathrm{b}}_{\mathrm{BI}} & \mathbf{C}^{\mathrm{b}}_{\mathrm{BB}} \end{bmatrix} \begin{bmatrix} \dot{\mathbf{x}}^{\mathrm{b}}_{\mathrm{I}} \\ \dot{\mathbf{x}}_{\mathrm{B}} \end{bmatrix} + \begin{bmatrix} \mathbf{K}^{\mathrm{b}}_{\mathrm{II}} & \mathbf{K}^{\mathrm{b}}_{\mathrm{IB}} \\ \mathbf{K}^{\mathrm{b}}_{\mathrm{BI}} & \mathbf{K}^{\mathrm{b}}_{\mathrm{BB}} \end{bmatrix} \begin{bmatrix} \mathbf{x}^{\mathrm{b}}_{\mathrm{I}} \\ \mathbf{x}_{\mathrm{B}} \end{bmatrix} = \begin{bmatrix} \mathbf{f}_{\mathrm{ext,I}} \\ \mathbf{f}_{\mathrm{ext,B}} + \mathbf{f}_{\mathrm{tb}\to\mathrm{b}} \end{bmatrix} \tag{1a}$$

$$\begin{bmatrix} \mathbf{M}_{\mathrm{II}}^{\mathrm{tb}} & \mathbf{M}_{\mathrm{IB}}^{\mathrm{tb}} \\ \mathbf{M}_{\mathrm{BI}}^{\mathrm{tb}} & \mathbf{M}_{\mathrm{BB}}^{\mathrm{tb}} \end{bmatrix} \begin{bmatrix} \ddot{\mathbf{x}}_{\mathrm{I}}^{\mathrm{tb}} \\ \ddot{\mathbf{x}}_{\mathrm{B}} \end{bmatrix} + \begin{bmatrix} \mathbf{C}_{\mathrm{II}}^{\mathrm{tb}} & \mathbf{C}_{\mathrm{IB}}^{\mathrm{tb}} \\ \mathbf{C}_{\mathrm{BI}}^{\mathrm{tb}} & \mathbf{C}_{\mathrm{BB}}^{\mathrm{tb}} \end{bmatrix} \begin{bmatrix} \dot{\mathbf{x}}_{\mathrm{I}}^{\mathrm{tb}} \\ \dot{\mathbf{x}}_{\mathrm{B}} \end{bmatrix} + \begin{bmatrix} \mathbf{K}_{\mathrm{II}}^{\mathrm{tb}} & \mathbf{K}_{\mathrm{IB}}^{\mathrm{tb}} \\ \mathbf{K}_{\mathrm{BI}}^{\mathrm{tb}} & \mathbf{K}_{\mathrm{BB}}^{\mathrm{tb}} \end{bmatrix} \begin{bmatrix} \mathbf{x}_{\mathrm{I}}^{\mathrm{tb}} \\ \mathbf{x}_{\mathrm{B}} \end{bmatrix} = \begin{bmatrix} \mathbf{0} \\ -\mathbf{f}_{\mathrm{tb}\to\mathrm{b}} \end{bmatrix}, \tag{1b}$$

where $\mathbf{M}$, $\mathbf{C}$, and $\mathbf{K}$ correspond to the mass, damping and stiffness matrices, respectively. External forces $\mathbf{f}_{\mathrm{ext}}$ are applied to the uniform beam. The displacement is noted $\mathbf{x}$. The influence of mechanical ABH on the uniform beam is located on nodes B and is written $\mathbf{f}_{\mathrm{tb}\to\mathrm{b}}$. The rest of the nodes are denoted by the subscript I. Using the Laplace variable s, the ABH impedance can be obtained with Equation 1b

$$\mathbf{X}_{\mathrm{I}}^{\mathrm{tb}} = -\left(s^2\mathbf{M}_{\mathrm{II}}^{\mathrm{tb}} + s\mathbf{C}_{\mathrm{II}}^{\mathrm{tb}} + \mathbf{K}_{\mathrm{II}}^{\mathrm{tb}}\right)^{-1}\left(s^2\mathbf{M}_{\mathrm{IB}}^{\mathrm{tb}} + s\mathbf{C}_{\mathrm{IB}}^{\mathrm{tb}} + \mathbf{K}_{\mathrm{IB}}^{\mathrm{tb}}\right)\mathbf{X}_{\mathrm{B}} = \mathbf{Z}_{\mathrm{IB}(s)}\mathbf{X}_{\mathrm{B}} \tag{2a}$$

$$-\mathbf{F}_{\mathrm{tb}\to\mathrm{b}} = \left[\left(s^2\mathbf{M}_{\mathrm{BI}}^{\mathrm{tb}} + s\mathbf{C}_{\mathrm{BI}}^{\mathrm{tb}} + \mathbf{K}_{\mathrm{BI}}^{\mathrm{tb}}\right)\mathbf{Z}_{\mathrm{IB}}(s) + \left(s^2\mathbf{M}_{\mathrm{BB}}^{\mathrm{tb}} + s\mathbf{C}_{\mathrm{BB}}^{\mathrm{tb}} + \mathbf{K}_{\mathrm{BB}}^{\mathrm{tb}}\right)\right]\mathbf{X}_{\mathrm{B}} = \mathbf{Z}_{\mathrm{ABH}}(s)\,\mathbf{X}_{\mathrm{B}} \tag{2b}$$

where $\mathbf{X}_{\mathrm{I}}^{\mathrm{tb}}$, $\mathbf{X}_{\mathrm{B}}$, and $\mathbf{F}_{\mathrm{tb}\to\mathrm{b}}$ are the Laplace transforms of $\mathbf{x}_{\mathrm{I}}^{\mathrm{tb}}$, $\mathbf{x}_{\mathrm{B}}$, and $\mathbf{f}_{\mathrm{tb}\to\mathrm{b}}$, respectively. From Equation 2b, it becomes clear that the exact ABH effect can be reproduced if one measures all the displacement and rotations at the tip of the beam ($\mathbf{X}_{\mathrm{B}}$) and applies to the same location the forces and torques $\mathbf{F}_{\mathrm{tb}}$. This can be very challenging to realize in practice. To simplify the problem, only the rotational part of the ABH, $\mathbf{Z}_{\mathrm{ABH},\phi}$, will be modeled.

2.2. Implementation through piezoelectric patches

In the system presented in Figure 2, the beam is constituted by a set of sensors (providing the relative displacement between the boundaries of the piezoelectric patches) and by a set of actuators (applying to the boundaries of the patches an opposite torque). The equations of motion of the second system in Figure 2 reads

$$\begin{cases} \mathbf{M}\ddot{\mathbf{x}} + \mathbf{C}\dot{\mathbf{x}} + \mathbf{K}_{\mathrm{sc}}\mathbf{x} + \sum_{i=1}^{N}\left(\mathbf{\Theta}_i C_p V_{i,\mathrm{a}}\right) &= \mathbf{f}_{\mathrm{ext}} \\ \mathbf{\Theta}_i^{\intercal}\mathbf{x} - \left(C_p\right)^{-1} q_{i,\mathrm{a}} = V_{i,\mathrm{a}}, & \forall i \in [\![1,N]\!] \\ C_p\mathbf{\Theta}_i^{\intercal}\mathbf{x} = q_{i,\mathrm{s}}, & \forall i \in [\![1,N]\!], \end{cases} \tag{3}$$

where $V_{i,\mathrm{a}}$ and $q_{i,a}$ correspond to the voltage and charge of the $i-$th actuator respectively. The scalar $q_{i,\mathrm{s}}$ represents the charge of the $i-$th sensor. The scalar C_p represents the capacitance at constant strain of a piezoelectric patch. The matrix $\mathbf{\Theta}_i$ is the ith piezoelectric coupling vector, assumed to be identical for both the actuator and sensor. For better readability, the superscript and subscript have been omitted in the equations as only the uniform beam is considered here. Although Figure 2 displays a single set of patches at an arbitrary location, the derivations presented in Section 1, showed that to obtain the rotational ABH effect, one must retrieve the rotation at the tip of the beam and apply a specific torque at the same location. Hence, to retrieve the ABH effect, the piezoelectric patches must cover the entire length of the beam and must be connected in parallel [12]. Equations 3 were derived assuming that N patches are used to cover the beam. The choice of N does not affect the derivations (the length of the patches is chosen such that their length is equal to the length of the beam divided by N).

To ensure a collocated system [13] and to ensure the rotational effect of the ABH, two piezoelectric patches are paired to form either an actuator or a sensor cell (see Figure 2). In the equations, this choice only impacts the matrix $\mathbf{\Theta}_i$ for which only its rotational components are non-zeros, noted γ. A synthesized impedance is programmed between the voltage and the measured current,

$$V_{\mathrm{a}} = Z(s)\,q_{\mathrm{s}}. \tag{4}$$

Complete derivations are provided in [12] and gives the following result

$$Z(s) = -\frac{\mathbf{Z}_{\mathrm{ABH},\phi}}{\left(C_p\gamma\right)^2}. \tag{5}$$

Although these derivations show that the exact rotational ABH effect can be reproduced with the synthesized impedance, covering the entire system with piezoelectric patches is hardly practical. In many studies, the concept of ABH-featured resonant beam damper [14] is employed and demonstrated that the mechanical ABH does not need to be placed at the boundary of the system to be effective. To obtain a practical system, the following experimental section uses this approach and considers a few piezoelectric cells located near the clamping side to apply the VABH effect.

3. EXPERIMENTAL DEMONSTRATION

The experimental setup is depicted in Figure 3. A one-meter long uniform beam is tested (all the information about the material, geometry and so on can be found in [12]). The piezoelectric patches are connected to electrical circuits to adapt the voltages and current coming in and out of the patches.

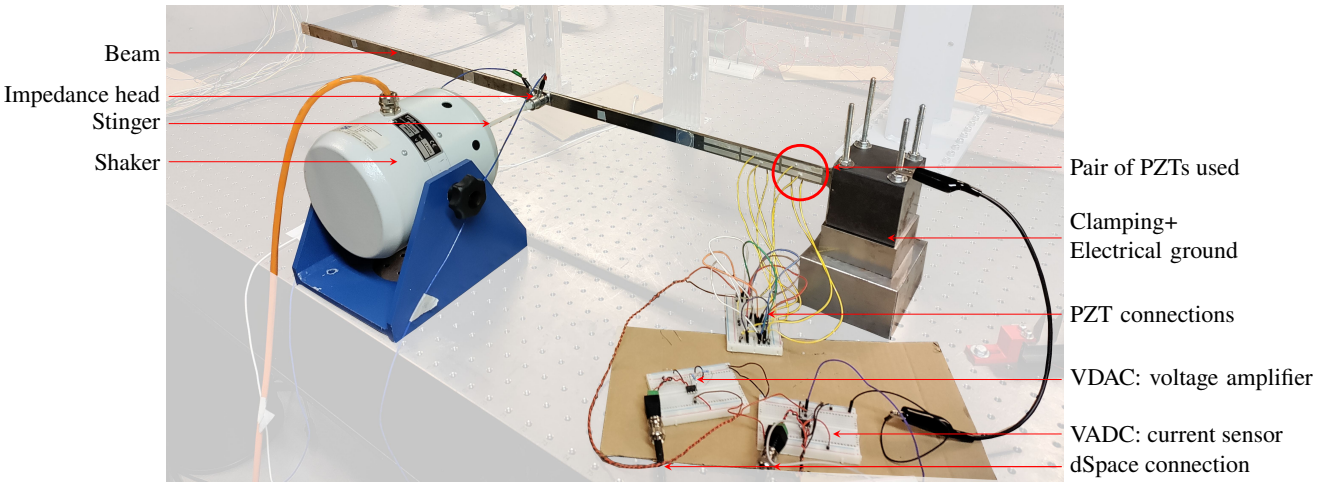

Figure 3: Experimental cantilever beam equipped with piezoelectric patches and a shaker.

The first seven resonance frequencies of the uniform beam are listed in Table 1. As the amplitude of the first resonance is very low, only the others modes will be mitigated.

Table 1: Resonance frequencies of the uniform beam.

Number of the modes	**Resonance frequency** (Hz)
1	5
2	31.5
3	89.5
4	176
5	283.5
6	595
7	816.5

As underlined in the introduction, the concept of VABH offers the unique possibility to model any mechanical ABH: any length, material, power law, etc can be considered [11]. In this work, the VABHs were chosen to be made of steel with the same width as the uniform beam and a power law equal to 2. The considered VABHs differ from one another with respect to their lengths: 100 cm for VABH 1, 70 cm for VABH 2, 50 cm for VABH 3, and 40 cm for VABH 4.

To ensure the stability of the system at high frequencies, the synthesized impedance (see Equation 5) is multiplied by a low-pass filter whose cut-off frequency is around 1 kHz. Figure 4 presents the experimental results for the VABH 2, 3, and 4. With VABH 2, all the peaks except the last one are attenuated by at least 4 dB. The other VABHs do not present systematic vibration reduction: for example the peak at 31 Hz does not get attenuated, on the contrary, a small amplification is observed for VABH 4. However, VABHs 3 and 4 give higher attenuation for some peaks: for the resonant mode at 176 Hz, VABH 4 has a 25 dB reduction against 20 dB for VABH 2. These observations are consistent with the length of the chosen VABHs. Indeed, VABH 2 has a longer length than VABH 4, hence, for lower frequencies, it is expected to have better vibration mitigation.

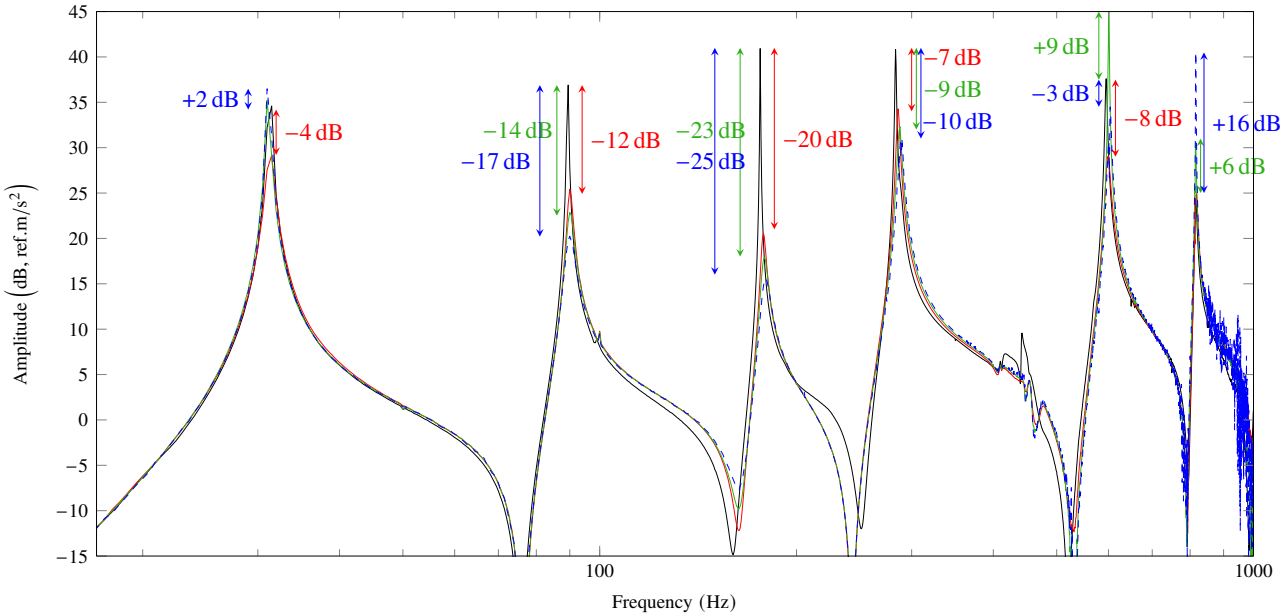

Figure 4: FRF with one PZT cell (accelerance at the shaker location). (—): plant, (—): L_{ABH} = 700 mm, (—): L_{ABH} = 500 mm, and (—): L_{ABH} = 400 mm.

Figure 5 presents the results of the VABH 3 with different values of the gain for the controller. As expected, the larger the gain, the better the vibration reduction. At high frequencies (for the last peak), an amplification is obtained. This result comes from the coupling between the controller and the low-pass filter.
Finally, Figure 6 shows the results of VABH 1, 2, and 3 when a special tuning of the low-pass filter and the gain value was made for each controller. Their respective gain is equal to 1, 1.5, and 2. Due to its higher gain than VABH 1, VABH 2 has a higher vibration attenuation for the considered frequency range. A similar trend is observed for VABH 3 except for the first and last peaks.

4. CONCLUSION

The theoretical concept of the VABH was presented as well as its first experimental application. The results showed overall very good vibration reduction. For one case, a reduction of at least 7 dB was obtained in the frequency range [10 Hz, 1000 Hz]. The results were obtained with only 4 piezoelectric patches located near the clamped side of the uniform beam. These results obtained for a compact design are very promising for future applications.

ACKNOWLEDGEMENTS

Samuel Quaegebeur is thankful for the financial support of the ANR (project ANR-22-CPJ2-0061-01). This work was also supported by the Fonds de la Recherche Scientifique - FNRS under Grant n° [FRS-FNRS PDR T.0124.21], which is gratefully acknowledged. Li Cheng also thanks the support

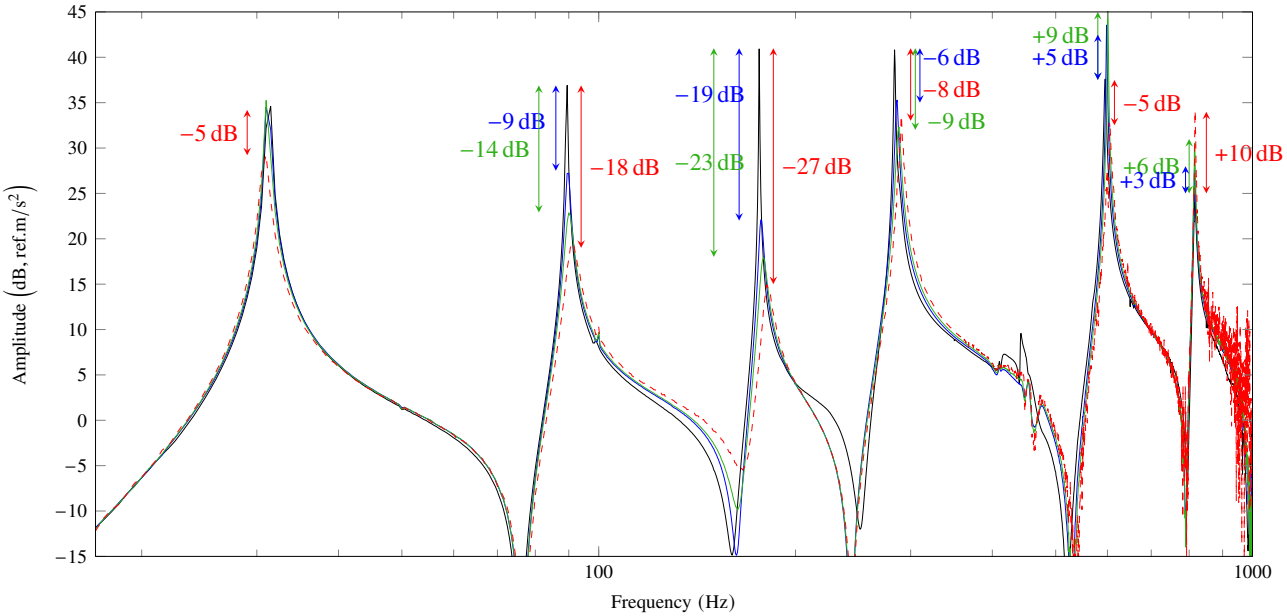

Figure 5: FRF for VABH 3 with different gain values. (—): plant, (—): gain of 2, (—): gain of 1, and (—): gain of 0.5.

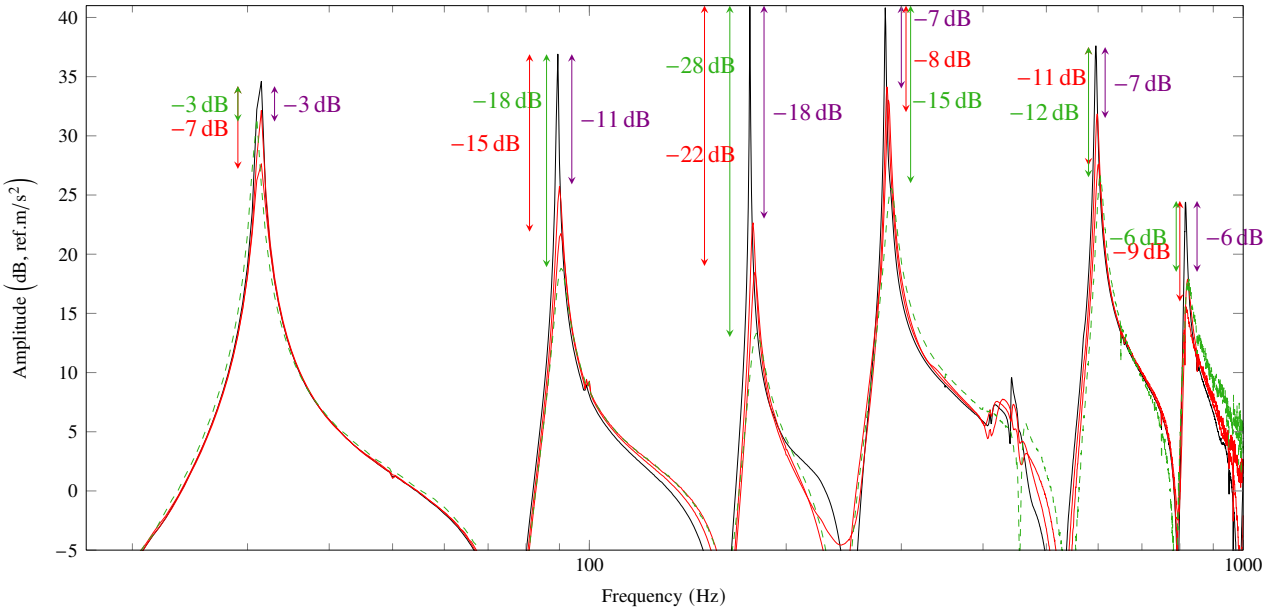

Figure 6: FRF with low-pass filter tuning. (—): plant, (—): $L_{\mathrm{ABH}} = 1000\,\mathrm{mm}$, (—): $L_{\mathrm{ABH}} = 700\,\mathrm{mm}$, and (—): $L_{\mathrm{ABH}} = 500\,\mathrm{mm}$.

from the Research Grant Council of the Hong Kong SAR (PolyU 152023/20E).

REFERENCES

1. M. Mironov. Propagation of a flexural wave in a plate whose thickness decreases smoothly to zero in a finite interval. *Sov. Phys. Acoust.*, 34:318–319, January 1988.
2. O. Aklouche, A. Pelat, S. Maugeais, and F. Gautier. Scattering of flexural waves by a pit of quadratic profile inserted in an infinite thin plate. *Journal of Sound and Vibration*, 375:38–52, August 2016.
3. A. Pelat, F. Gautier, S.C. Conlon, and F. Semperlotti. The acoustic black hole: A review of theory and applications. *Journal of Sound and Vibration*, 476:115316, June 2020.

4. L. Tang and L. Cheng. Enhanced Acoustic Black Hole effect in beams with a modified thickness profile and extended platform. *Journal of Sound and Vibration*, 391:116–126, March 2017.
5. J.Y. Lee and W. Jeon. Vibration damping using a spiral acoustic black hole. *The Journal of the Acoustical Society of America*, 141(3):1437–1445, March 2017. Publisher: Acoustical Society of America.
6. H. Li, C. Touzé, A. Pelat, and F. Gautier. Combining nonlinear vibration absorbers and the Acoustic Black Hole for passive broadband flexural vibration mitigation. *International Journal of Non-Linear Mechanics*, 129:103558, March 2021.
7. H. Li, M. Sécail-Géraud, A. Pelat, F. Gautier, and C. Touzé. Experimental evidence of energy transfer and vibration mitigation in a vibro-impact acoustic black hole. *Applied Acoustics*, 182:108168, November 2021.
8. X. Sun, G. Kerschen, and L. Cheng. Energy transfer for enhanced acoustic black hole effect through a cable-induced mechanical nonlinearity. *International Journal of Non-Linear Mechanics*, 161:104682, May 2024.
9. J. Cheer, K. Hook, and S. Daley. Active feedforward control of flexural waves in an Acoustic Black Hole terminated beam. *Smart Materials and Structures*, 30(3):035003, January 2021. Publisher: IOP Publishing.
10. L. Zhang, G. Kerschen, and L. Cheng. Electromechanical Coupling and Energy Conversion in a PZT-Coated Acoustic Black Hole Beam. *International Journal of Applied Mechanics*, 12(08):2050095, September 2020. Publisher: World Scientific Publishing Co.
11. S. Quaegebeur, G. Raze, L. Cheng, and G. Kerschen. A virtual acoustic black hole on a cantilever beam. *Journal of Sound and Vibration*, 554:117697, June 2023.
12. S. Quaegebeur, G. Raze, L. Cheng, and G. Kerschen. Realization of an autonomous virtual acoustic black hole with piezoelectric patches. *Smart Materials and Structures*, 33(2):025022, January 2024. Publisher: IOP Publishing.
13. A. Preumont. Collocated versus Non-collocated Control. In A. Preumont, editor, *Vibration Control of Active Structures: An Introduction Third Edition*, Solid Mechanics and Its Applications, pages 117–130. Springer Netherlands, Dordrecht, 2011.
14. T. Zhou and L. Cheng. A resonant beam damper tailored with Acoustic Black Hole features for broadband vibration reduction. *Journal of Sound and Vibration*, 430:174–184, September 2018.